

A model study of global variability in mesospheric cloudiness

David E. Siskind*, M.H. Stevens, C.R. Englert

Naval Research Laboratory, E.O. Hulburt Center for Space Research, Code 7641, Washington, DC 20375, USA

Received 3 June 2004; received in revised form 13 September 2004; accepted 16 November 2004

Available online 24 January 2005

Abstract

We have performed microphysical calculations of mesospheric cloudiness which are driven by output (vertical wind, water vapor mixing ratio and temperature) from a two-dimensional (2D) global chemical/dynamical model. The variations in the 2D model output drive variations in the simulated clouds which can be compared with cloud observations. The specific cloud observables we model are ice content, altitude, peak backscatter at 532 nm and albedo at 252 nm. We categorize these parameters in terms of their variations with latitude, solar activity and hemisphere (north vs. south). In agreement with observations, we find brighter clouds in the Northern Hemisphere (NH) relative to the south and at solar minimum relative to solar maximum. Also we find that cloud altitudes are higher in the Southern Hemisphere (SH) relative to the NH. Quantitatively, compared with observations, it appears that the model may overstate the magnitude of these variations. Thus, the entire range of observed cloud altitudes, poleward of 65–70°, is about 2 km (83–85 km), whereas the range in the calculated heights range extends up to 5 km (83–88 km). In addition, the calculated solar cycle brightness change of up to an order of magnitude appears larger than the limited available observations. Since the model H₂O variation in the 80–90 km region with respect to solar activity is relatively small (10–40%), it is not the cause of our large model cloud variability. Rather, for both hemispheric variation and solar cycle changes, we suggest that the model temperature variability may be too great.

Published by Elsevier Ltd.

Keywords: Middle atmosphere; Solar cycle; Microphysics; Mesopause

1. Introduction

Since the late 19th century, mesospheric clouds have captured the interest of aeronomers for several reasons. First, they occur in one of the most extreme conditions of the earth's atmosphere: the very cold summer mesopause. Second, there is the continued speculation that the very existence of these clouds is due to anthropogenic influences on middle atmospheric composition and climate (Thomas et al., 1989; Thomas, 1996), although this is controversial (e.g. von Zahn, 2003).

Historically, most of the measurements of these clouds have been from Northern Europe or Canada, via ground-based observatories. In this manifestation, they have been known as noctilucent clouds (NLCs) (Fogle and Haurwitz, 1966; von Cossart et al., 1999; Lübken et al., 1996). In the last 30 years, these observations have been expanded to include ground-based measurements from Antarctica (Chu et al., 2001) as well as global satellite-based data (Thomas, 1991; DeLand et al., 2003). Thomas (1991) advocated the term polar mesospheric clouds (PMCs) to emphasize the global nature of these clouds and that is the term we use here.

Early measurements from the Solar Mesosphere Explorer (SME) (Thomas and Olivero, 1989) showed

*Corresponding author.

E-mail address: siskind@uap2.nrl.navy.mil (D.E. Siskind).

the existence of a well-defined season for PMC formation that was linked to the existence of the cold summer mesopause. In addition, SME data showed that clouds occurred more frequently at higher latitudes; this is generally attributed to lower temperatures as one approaches the summer pole (Thomas, 1991). Modeling studies have confirmed that MC formation depends sensitively on the climate of the high latitude summer mesopause region. Thus, observations of these clouds can provide constraints on more general properties of the atmosphere.

For example, one important PMC diagnostic is the altitude at which they are observed. Chu et al. (2001, 2003) have recently presented data and a model analysis which indicated that mesospheric clouds over the South Pole (SP) were at a higher altitude than in the Northern Hemisphere (NH). This would appear to contradict the results of Carbary et al. (1999), who found PMCs to be at the same altitude worldwide. If PMCs are truly higher over the SP, it suggests a difference in mesospheric climates between the NH and the Southern Hemisphere (SH) perhaps in the temperature. Differences in temperature and/or the water vapor abundance might also be the cause of variability in the frequency of PMC occurrence reported by several satellites. The suggestion of a warmer (or dryer) SH mesopause region might be inferred from the dimmer and less frequent clouds seen in the SH according to satellite data (DeLand et al., 2003; Hervig et al., 2003). Woodman et al. (1999) made this argument to explain the relative paucity of SH Polar Mesospheric Summer Echoes (PMSE), a phenomena related to PMCs. However, the question of north–south (N–S) mesopause temperature differences has been the subject of debate as Lübken et al. (1999) reported little difference in the Antarctic summer mesopause temperature as compared with similar data taken in the Arctic.

Recently, Siskind et al. (2003) (hereinafter S03) published an analysis of two-dimensional (2D) model results (from the NRL two-dimensional chemical/dynamical model of the middle atmosphere (CHEM2D) model), which supported the idea of a warmer SH summer mesopause. This conclusion was based upon the effects of relatively well-documented N–S differences in the summer climates of the underlying stratosphere and troposphere on gravity wave propagation to the mesosphere. They suggested that their results implied fewer and weaker PMCs and PMSEs in the SH relative to the NH. Earlier, Garcia (1989) suggested that a solar cycle should exist in mesospheric clouds with fewer clouds at solar maximum when H₂O photodissociation should peak. However, neither modeling study quantified what those differences would be; that would have required a microphysical model capable of translating the calculated differences in mesopause climate into cloudiness differences. In the present paper, we do just that, i.e. we use a microphysical model driven by output from

CHEM2D to more precisely quantify the expected N–S differences in mesospheric cloudiness and in the variability of that cloudiness. Our results can both validate the CHEM2D simulations as well as provide testable hypotheses suitable for observational verification.

2. Model approach

Our overall approach is to use a CHEM2D to specify the atmospheric basic state. The relevant outputs, H₂O, vertical wind (w^*) and temperature (T) are then used to drive a one-dimensional (1D) version of the Community Aerosol Radiation Model for Atmospheres (CARMA). Currently, there is no feedback from the microphysical results on the CHEM2D model; this is planned for future work. These models are described in more detail below.

The CHEM2D model and its application to the study of the summer mesopause was most recently described by S03. Since that work, we have incorporated two major changes to the model. First, the model top was extended up to 125 km ($p_{\min} = 2.5e - 5$ mbar), from about 105 km ($p_{\min} = 2e - 4$ mbar). Raising the top altitude increases our confidence in calculating winds and temperatures in the 90–105 km region. Second, we use new heating and cooling algorithms. For the mesosphere, we now use the code of Fomichev et al. (1998). This code has the advantage of allowing any value for the CO₂ mixing ratio and thus allows for a self-consistent calculation of the cooling rate with the model CO₂ densities. We still retain the detailed ozone heating rate calculation which is identical to the O₃ and O₂ dissociation rate calculation in the photochemical package. However, previously we used the diurnally averaged ozone to calculate the radiative heating; now we more properly use the daytime ozone (obtained by applying a precalculated night-to-day ratio from a 1D diurnal model). Since daytime mesospheric ozone is lower than the diurnal average, this means less heating and lower mesospheric temperatures than in S03. For the stratosphere, we use the CLIRAD scheme (Chou et al., 2001; Chou and Suarez, 2002; see also McCormack, 2003) for both heating and cooling. In this implementation, the stratospheric and mesospheric radiative schemes are merged using a weighted average between 30 and 50 km (note that this is 20 and 40 km in McCormack, 2003).

So that the model better simulates the PMC altitudes and brightness, we made some small changes to the gravity wave drag parameterization of S03. Specifically, by lowering the launch amplitudes of the waves given in Table 1 of S03, we raised the altitudes at which they saturate and break. We “tuned” the gravity wave amplitudes until the CARMA model produced clouds

between 82 and 84 km at 71°N. This is because one of the most robust observational characteristics of PMCs is their altitude over Andoya at 69°N (von Zahn et al., 1998; Lübken et al., 1996). No tuning was done for other locations and conditions; any differences in calculated cloud properties will be discussed in terms of the relevant physics and dynamics of the models. This change and the other CHEM2D changes described above also changed some of the relevant output (w^* , T , H_2O) for PMC modeling and will be discussed further below and in the next section. The CHEM2D output is used as input to drive the CARMA microphysical model (Rapp et al., 2002). With the exception of the CHEM2D input, our adaptation of CARMA is the same as that described recently by Stevens et al. (2004). For this work, the key results from CARMA are the ice equivalent mixing ratio ($H_2O(\text{ice})$), the perturbed water vapor and the particle size. In addition, we use Mie theory (Bohren and Huffman, 1983) to calculate the cloud albedo at 252 nm which can be compared with satellite data (DeLand et al., 2003; Stevens et al., 2004) and the backscatter ratio (BSR) at 532 nm which corresponds to typical ground-based data (e.g. Fiedler et al., 2003).

The results in this paper come from two CHEM2D simulations, one for solar maximum and one for solar minimum conditions. The solar flux we use comes from the SEP86 (solar min) and NOV89 (solar max) reference spectra given by Lean et al. (1997). For the 180–200 nm wavelength region, we assume roughly a 9–11% change from solar maximum to minimum, and for Lyman alpha, we assume a variation from $3.0 \times 11 \text{ ph/cm}^2/\text{s}$ at solar minimum to $5.5 \times 11 \text{ ph/cm}^2/\text{s}$ at solar maximum.

In the past (S03), we have used pressure altitude ($Z^* = -7 \ln(p/1000)$). This assumes a constant 7 km scale height which is not valid in the cold summer mesopause region where scale heights shrink to less than 5 km. Thus, differences between pressure altitudes and real geometric altitudes will be magnified in this region. Since PMC occurrences are generally referenced to geometric altitudes and we wish to focus specifically on comparisons with observed cloud heights, we have converted the model pressure altitudes to geometric altitudes using the model temperature profile and assuming the pressure at the surface is 1000 mbar. In doing this conversion, we assumed a constant mean molecular weight with altitude but accounted for the variation of gravity with altitude. This effect makes about a 1 km difference in the calculated mesopause altitude.

3. Model results

3.1. CHEM2D results

For each of our two CHEM2D simulations (solar max and solar min), we sample the output at eight

latitudes, approximately 85°S, 80°S, 75°S, 71°S, and the equivalent for the NH. With a CHEM2D latitudinal resolution of 4.86°, the 85° grid point is the highest in the model. The 71–85° latitude range corresponds to the range where clouds are generated in our model and also to the latitude range of routine cloud and summer mesopause climate observations (e.g. Andoya at 69°N, Svalbard, 78°N, Rothera, 67°S and the South Pole (SP)). We will only show model results for Day 181 (NH) and Day 361 (SH). The seasonal cycle of mesopause temperatures may be affected by the presence of clouds and a detailed study of this effect is deferred for future work.

Fig. 1 shows the calculated temperature profiles for the days and latitudes discussed above for solar maximum (Fig. 1a) and solar minimum (Fig. 1b) conditions. While the absolute value of the mesopause temperature minima are about 10–20 K lower than S03, the relative variations (i.e. latitudinal variation, N–S asymmetry) are qualitatively the same. The figure shows that the coldest temperatures are at the North Pole (NP) at solar minimum with NH temperatures all lower than their SH counterparts below 90 km. Compared to observations, our model results are generally in good agreement. Our 70°N mesopause minima of 127 K (solar min) and 133 K (solar max) agree well with the 129 K of Lübken (1999). Note that a clear observation of solar cycle variation in summer mesopause temperatures has never been made. This is probably due to limited data; however, it may also be because such variations are smaller in the atmosphere than in our model and thus relatively harder to detect. We will return to this point later.

The 70°S mesopause minima of 132 K (solar min) and 137 K (solar max) are also in general agreement with Lübken et al. (1999) in terms of absolute magnitude. Our 70°S mesopause temperatures are about 6 K higher than at 70°N, while Lübken et al. argue that within their experimental error, there is little or no difference between NH and SH summer mesopause temperatures. On the other hand, Pan and Gardner (2003) report significantly higher mesopause temperatures in the southern summer, rarely falling below 140 K at the SP. This would imply a huge NH–SH asymmetry of order 20 K. Clearly, a consensus has not yet been reached on N–S temperature differences in the summer mesosphere.

In terms of the latitude variation, our prediction of decreasing temperatures going toward the poles is consistent with Fig. 2 of Chu et al. (2004) for the SH. While there is no NP data, the data from Svalbard at 78°N (Lübken and Mullemann, 2003) are consistent with a colder, higher altitude mesopause as one proceeds polewards from 69°N (Lübken, 1999). Also, its worth noting that these latitude and altitude trends in our 2D mesopause are very similar to those seen in the three-dimensional (3D) model calculations of von Zahn and Berger (2003).

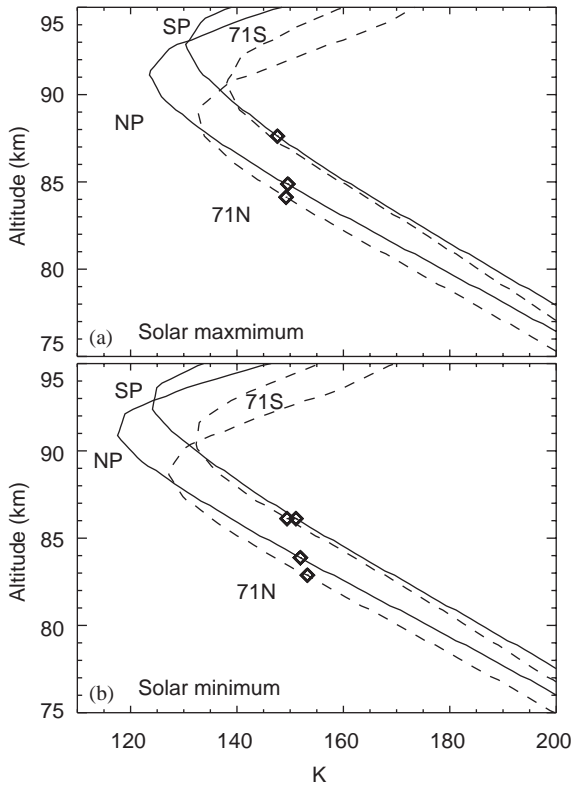


Fig. 1. CHEM2D temperature profiles for four latitudes (71°N, 85°N, 71°S and 85°S) and for solar maximum (a) and solar minimum (b) conditions. The SH profiles are for Day 361, the NH profiles are for Day 181. The altitude profiles are geometric altitudes calculated using the model pressure/temperature profile (see text). The solid lines labeled NP (North Pole) and SP (South Pole) refer to the model output at 85°. The dashed lines are for 71°. The diamonds are marked at the altitude of the maximum ice content according to Fig. 6. Only three diamonds are shown in (a) because the model did not produce a cloud at 71°S at solar maximum.

Finally, the altitude difference between the heights of the NH and SH mesopauses is almost solely due to hydrostatic effects. In both hemispheres, the model polar summer mesopause is at the same model grid point, near .001 mbar. However, because the SH is warmer than the NH in summer at all altitudes in the middle atmosphere (e.g. Figs. 11 and 14 of S03), the .001 mbar surface is about 1.5–2 km higher in altitude in the SH relative to the NH.

Fig. 2 shows H₂O profiles for the same conditions as in Fig. 1. The most noticeable feature of Fig. 2 is that the model predicts more H₂O in the SH than in the NH. This is a consequence of the differing seasonal cycles of mesospheric tracers in the SH as compared to the NH. This was first discussed for H₂O by Summers et al.

(1997) and for NO by Siskind (2000). Briefly, the greater eddy diffusion in the SH winter leads to less dehydration in the SH mesosphere—the H₂O is diffused upwards. This means that more H₂O is available to be lofted upward during early summer.

Fig. 3 presents a clearer overview of the N–S differences in the H₂O fields for both winter and summer. Because the simulations shown here assume a higher altitude for the gravity wave breaking relative to S03, this has the effect of increasing the water vapor abundance above 90 km relative to Fig. 10 of S03. The figure shows more H₂O in the SH relative to the NH for both summer and winter. Thus, the SH PMC region (80–90 km) experiences 3.0–5.0 ppmv of H₂O, while the NH is only 2.0–3.0. Note that the figure presents water vapor fields for the beginning of the PMC season. Later in the season (February 1, August 1—not shown), the NH–SH differences become less as strong upwelling in the NH continues to increase the H₂O. However, it is also now clear from satellite observations (Hervig et al., 2003) that the H₂O abundances are perturbed by the effects of PMCs themselves and thus our model of mesopause H₂O must be considered incomplete. Rather, as emphasized by S03, these fields serve as a guide for the nascent H₂O fields that drive the MC microphysics. The relative differences we predict are more robust than the absolute values at any given altitude in Fig. 3.

Our model predicts a solar cycle difference in H₂O with a 10% change at 80 km and about a 40% change at 90 km. This change is significantly smaller than first postulated by Garcia (1989) (a factor of 2–3 at 85 km for approximately the same change in solar flux). We attribute the difference mainly to the faster dynamics, associated with the lower temperatures, in our model relative to his. Our vertical winds (not shown) peak at 8 cm/s at the NP, in agreement with recent 3D results of Berger and von Zahn (2002); Garcia's peak is at about 4 cm/s. Faster dynamics mean that the effects of photochemical loss are inhibited relative to dynamical replenishment from lower altitudes where solar effects are smaller. Note that our overall H₂O abundance of 2–5 ppmv in the 80–90 km region is much greater than the 0.5–2.0 ppmv amounts Garcia shows in his Fig. 11, consistent with more vigorous upwelling in our model.

Fig. 4 shows the solar cycle variation in H₂O in units of percent difference, for a solstice case (Day 181, Fig. 4a) and an equinox case (Day 271, Fig. 4b). These figures show that, for a given altitude, the solar change in the summer polar region is the smallest relative to other latitudes and seasons. At equinox, the H₂O change is much larger—about 50% at 85 km. Marsh et al. (2003) presented an analysis of Halogen Occultation Experiment (HALOE) data at .0023 mbar (roughly 74 km in Fig. 4). Although their analysis focused on trends, it is possible to discern an approximate 20%

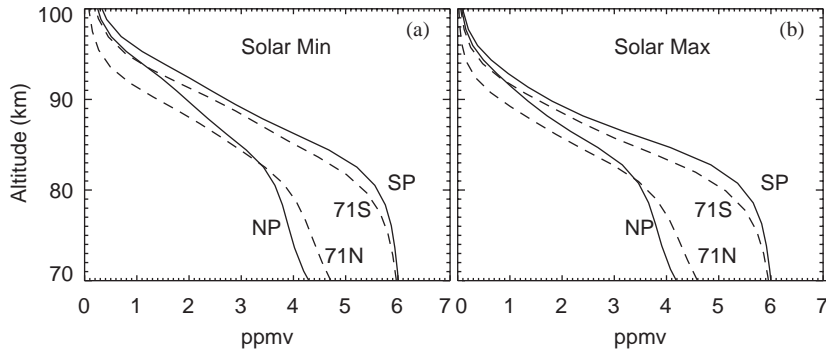


Fig. 2. Same as Fig. 1, but for H₂O profiles.

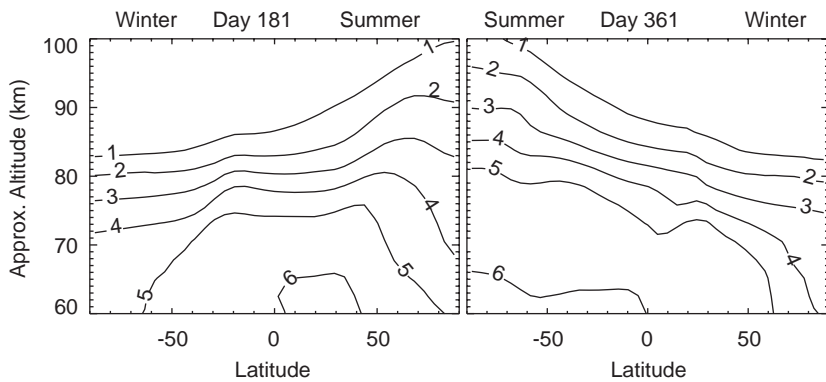


Fig. 3. Model H₂O contours (units are ppmv) for solar minimum conditions, Days 181 and 361. Here, unlike Figs. 1 and 2, the vertical scale is pressure altitude which assumes a constant scale height.

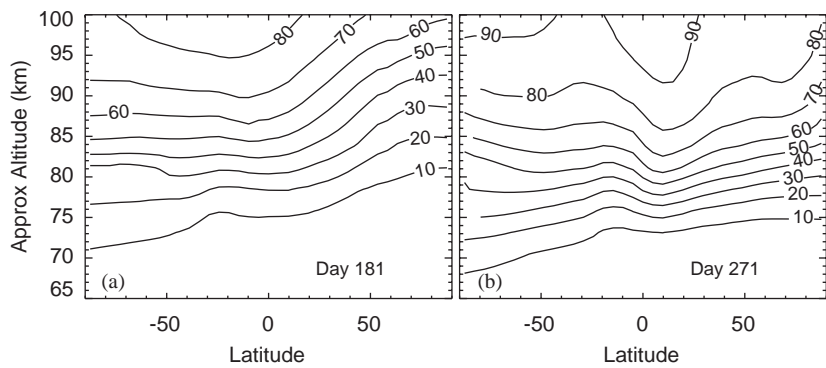


Fig. 4. Calculated (from CHEM2D) solar cycle percentage change in H₂O, defined as $100 * (\text{min} - \text{max}) / \text{min}$. Left panel: Day 181 (a solstice case); right panel: Day 271 (an equinox case).

solar cycle change in their data which, due to sampling considerations, is heavily weighted toward equinox conditions. This agrees well with the 10–15% change seen in Fig. 4 at 74 km, and thus we feel confident that our relatively small summer polar mesopause change is likely to be realistic.

3.2. CARMA results

We have run the CARMA model for the four latitudes, two solar cycle conditions and two hemispheres presented in Section 3.1 above, a total of 16 calculations. The model was initialized with the T , H₂O

and w^* from CHEM2D and integrated forward for 4 model days. A sample of the time-dependent output of CARMA is given in Fig. 5 for $\text{H}_2\text{O}(\text{ice})$ (Fig. 5a), water vapor (5b) and mean particle radius (5c) for solar minimum at 71°N . As shown in the figure, it takes about 1 day for a stable ice layer to form. However, the solution never really reaches a steady state. After the initial condensation/sedimentation period, an ice cloud forms at 83 km and persists for about 24 h. It then partially disappears for about 18 h, only to reappear by Day 3. Throughout this period, water vapor continues to build up at the base of the cloud layer. Also the mean particle size shows a general increase, going from 40 nm on Day 1 to over 60 nm for Days 2–4. A cyclical behavior of the ice clouds is undoubtedly due to the feedback between ice sedimentation and sublimation, followed by upwelling of the gas phase water vapor back into the cold region. A similar cyclical pattern was discussed by Sugiyama et al. (1996). The non-stationary behavior seen here illustrates the difficulty in choosing the proper part of the cloud lifecycle to compare with observations. Stevens et al. (2004), using reasonable estimates for the meridional wind, v^* , have argued that meridional transport time scales for PMC transport are about 2–5 days. Clouds much older than this are likely to be advected out of the cloud region (see also Gadsden, 1998; Fig. 3). For these reasons, a 3-day average of the CARMA output (from 24–96 model hours) should provide a reasonable general estimate of the clouds which would form in a specified environment and this is the same approach taken by Stevens et al. (2004). However, we will also present model error bars to reflect the variation of the model output as a function of sample time. This will serve as one measure of the robustness of our results.

We will focus on four specific observable characteristics of the clouds. The first is the amount of water vapor contained in the ice clouds ($\text{H}_2\text{O}(\text{ice})$ in Fig. 5a). The second is the altitude of the clouds. As we have already noted, the relative changes in cloud altitude with respect to our 71°N “tie-down” point can be considered an accurate measure of various aspects of the model physics. The third and fourth are two measurements of the cloud brightness: the peak BSR at 532 nm and the nadir albedo at 252 nm. The BSR results can be compared with ground-based measurements and the UV albedo results can be compared with the Solar Backscatter Ultraviolet (SBUV) satellite data (DeLand et al., 2003). For these four quantities, our main interest is in latitude differences within a hemisphere, N–S differences and solar cycle differences. We will not model the seasonal evolution or overall absolute water ice budgets since that would more properly require an interactive, self-consistent ice-chemistry–dynamics calculation.

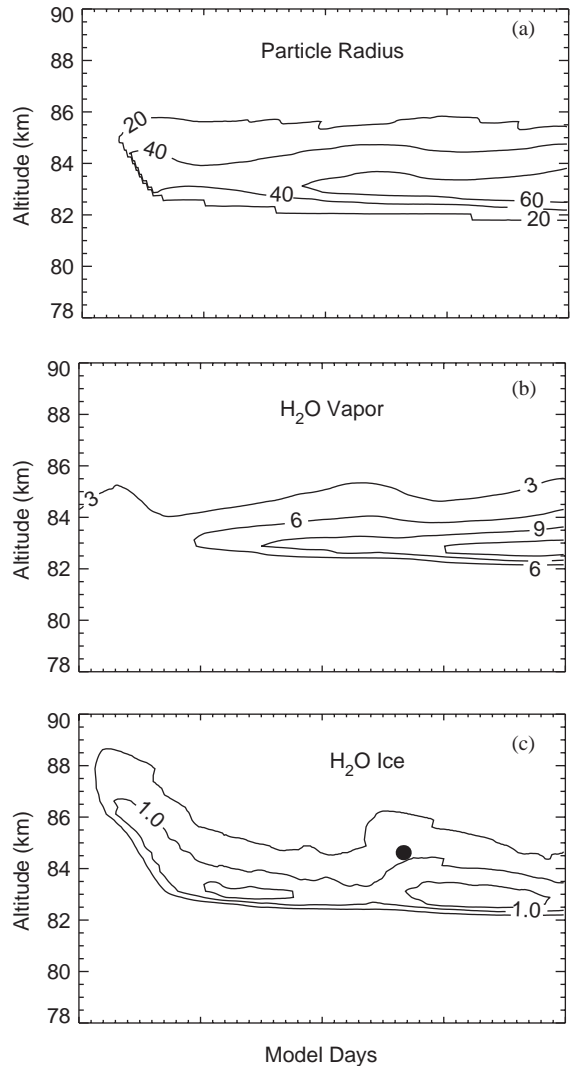


Fig. 5. Time-dependent results of the CARMA model for using inputs from the CHEM2D model for solar minimum, 71°N . The top panel is particle radius (in nm), calculated by taking the average radius, weighted by the particle number density in each bin. The middle panel is H_2O water vapor (in ppmv) and the bottom is the H_2O ice mixing ratio (in ppmv).

3.2.1. Ice content

Fig. 6 shows calculated profiles of $\text{H}_2\text{O}(\text{ice})$ for solar maximum (Fig. 6a) and solar minimum (Fig. 6b). Note that due to the warmer SH, the model does not produce a significant ice cloud at solar maximum at 71°N . Thus, Fig. 6a only shows three profiles, while Fig. 6b shows four. Fig. 6 clearly shows that more ice is contained in the clouds at solar minimum than at solar maximum. This follows primarily from the lower temperatures at solar minimum (i.e. the altitude of the 151–153 K isotherm is about 1 km lower) with a smaller

effect from the greater H₂O present at solar minimum. In general, more ice is present in the NH; even though in mixing ratio units, the ice abundance at the SP is greater than the NP ice peak. This is linked to the greater H₂O vapor available for condensation in the SH (i.e. Fig. 3); when the SH temperature is cold enough to consistently form clouds, they can contain as much or more H₂O than in the NH. In absolute density units, however, since the clouds are at a lower altitude in the NH (see below), the total number of H₂O molecules will be larger in the NH. As we will discuss, this leads to brighter clouds in the NH than in the SH.

Concerning solar cycle behavior, Fig. 6 shows that the solar cycle variation in ice abundance is smaller at the NP and much larger at the SP and 71°N (and arguably by an infinite amount at 71°S since there are no clouds there at solar max). This is because the temperatures at the NP are always consistently low enough for clouds to easily form. At 71°N and in the SH everywhere, the higher overall temperatures make cloud formation more problematic, especially at solar maximum, and thus more sensitive to a given change in temperature. This becomes more apparent when we consider the calculated cloud brightness.

3.2.2. Cloud altitude

Fig. 7 presents the peak altitude of the ice profile as a function of absolute latitude. The error bars represent the standard deviation of the calculated altitudes over the 24–96 h period in the CARMA simulation (see Fig. 5), weighted by the ice content at the cloud peak. A similar figure, using a compendium of observations, has been recently presented by Chu et al. (2004, their Fig. 4). Their figure shows 1–2 km higher clouds in the SH compared with their NH counterparts.

The N–S altitude differences can be directly linked to the altitude of the sublimation temperature. Referring

back to Fig. 1, the altitudes shown in Fig. 7 are marked as diamonds in the temperature profiles of Fig. 1. For solar minimum, the average temperature at the ice layer peak is about 153 K; for solar maximum, it is about 150 K. The small difference between these two values is due to the higher H₂O present at solar minimum which allows the clouds to persist at a slightly higher temperature. Taken together, these values are consistent with observations (Lübken et al., 1996) which have long shown the cloud layer to occur well below the altitude of the mesopause temperature minimum. Thus, the higher altitudes of the SH clouds are tied to the higher altitude of the 150–153 K isotherm, not the higher altitude of the SH mesopause. Note also that while the sense of the N–S altitude differences is correctly captured by the model, Fig. 7 appears to show a greater difference than what is observed. Thus, the SH clouds are about 3 km higher than their NH equivalents, whereas the observations cited above indicate an altitude difference closer to 1–2 km. This may mean that the model overestimates hemispheric differences and this will be discussed further.

Figs. 6 and 7 also show that the clouds at solar maximum are about 1 km higher than at solar minimum. While this appears to be a small effect and is often within the error bars of the calculations (also 1 km is less than the 2–2.5 km vertical resolution of the CHEM2D inputs to CARMA), it is qualitatively believable as a model result. It results from a combination of the small upward shift in the altitude of the 151–153 K isotherm at solar maximum, discussed above, and also a 20–30% decrease in cloud particle size at solar maximum (not shown) due, in part, to the reduced H₂O. The smaller clouds sediment more slowly and sublimate at higher altitudes than at solar minimum. There is a suggestion in Fielder et al. (2003) that this may actually occur. They found that the clouds they observed during the high solar activity years of 2000–2001 were about 1 km higher

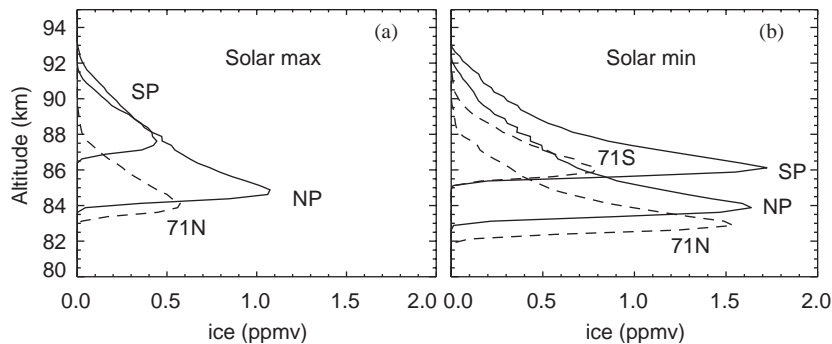


Fig. 6. Vertical profiles of the H₂O ice calculated by CARMA (a) for solar maximum and (b) for solar minimum. The profiles are an average of the last three days of the CARMA simulation (Days 1–4 in Fig. 5). Four latitudes are shown for solar minimum; only three are shown for solar maximum because the CHEM2D temperatures are too warm to permit cloud formation at 71°S at solar maximum. The identification of the curves is the same as in Figs. 1 and 2.

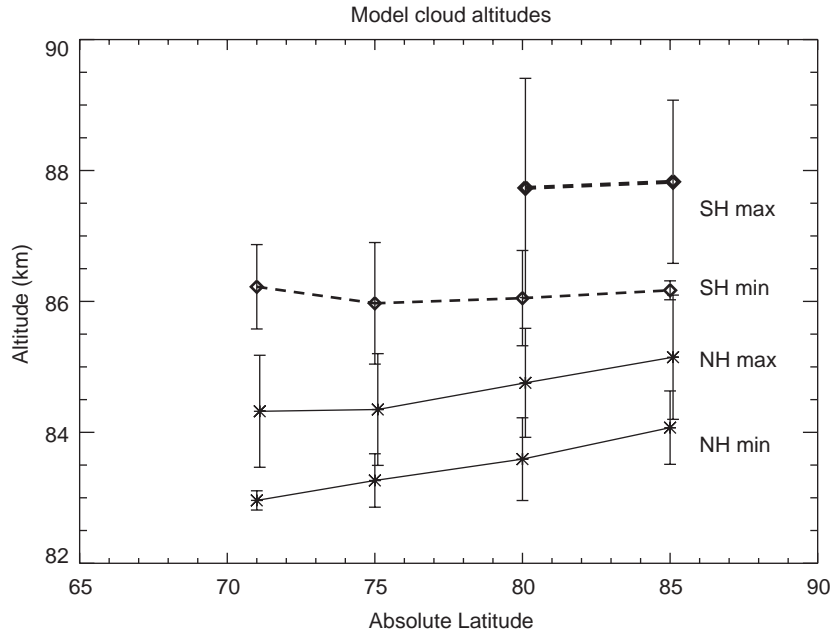


Fig. 7. Latitudinal and hemispheric variation in calculated PMC altitudes. As in Fig. 6, the altitudes are an average of Days 1–4 of each CARMA simulation. The error bars are the standard deviation of the calculated altitude, sampled every 6 h, and weighted by the equivalent ice mixing ratios (e.g. Fig. 5c). They serve to express the uncertainty in the model calculation due to uncertainties in cloud lifetimes.

than during the lower solar activity year of 1997 (see their Fig. 6b). While this clearly needs to be confirmed, we feel it makes physical sense and suggest that observers pursue this question.

Finally, Fig. 7 shows that in the NH, there appears to be a latitudinal variation with the NP clouds being 1 km higher than the 71°N clouds. While this latitude variation may be consistent with that shown by the data compiled by Chu et al. (2004), it is a less robust model result than, for example, the solar cycle change discussed above. Clearly, it results from a latitudinal change in the altitude of the 151–153 K isotherm. However, it is also sensitive to small changes in both the input H₂O fields as well as the temporal sampling of the CARMA output. For example, no latitudinal variation is seen in the height of the SH clouds. This topic would be better investigated with a version of CHEM2D that had much finer altitude resolution; such a model upgrade is not trivial, but is planned for the future.

3.2.3. Cloud brightness

Finally, we consider two measures of cloud brightness, the BSR at a visible wavelength (532 nm) and the albedo at an ultraviolet wavelength (252 nm). Fig. 8 shows the peak BSR – 1 at 532 nm. We choose to plot BSR – 1 rather than BSR because BSR – 1 is propor-

tional to β_{NLC} (von Cossart et al., 1999) and is analogous to the UV albedo in that it approaches zero as the cloud signal goes to zero. This wavelength was chosen because typical ground-based lidar measurements of NLCs are often made at 532 nm (e.g. Fiedler et al., 2003). The cloud brightness was calculated using standard Mie theory (Bohren and Huffman, 1983) and standard Rayleigh scattering for the background atmosphere. Particle densities and size distributions are taken from CARMA, which uses 35 size bins from 2 to 412 nm. The final result is an average over seven 12 h time steps between 1 and 4 days of the CARMA cloud simulation. Here, the error bars we show in the figure represent the extrema of the calculation rather than the standard deviation as in Fig. 7.

Fig. 8 shows that the NH clouds are much brighter relative to the SH than one might expect by looking at the ice profiles in Fig. 6. This is because the NH particles are calculated to be 20–30% larger than in the SH. Since cloud brightness varies as approximately (radius)⁶ but total ice content varies only as (radius)³, the brightness calculation increases the NH–SH asymmetry. There is also the tendency for greater solar cycle variation at subpolar latitudes (e.g. factor of 3 change at 85°N, 6–7 at 71°N) and in the SH. These are the more marginal conditions for cloud formation at these locations than at the NP.

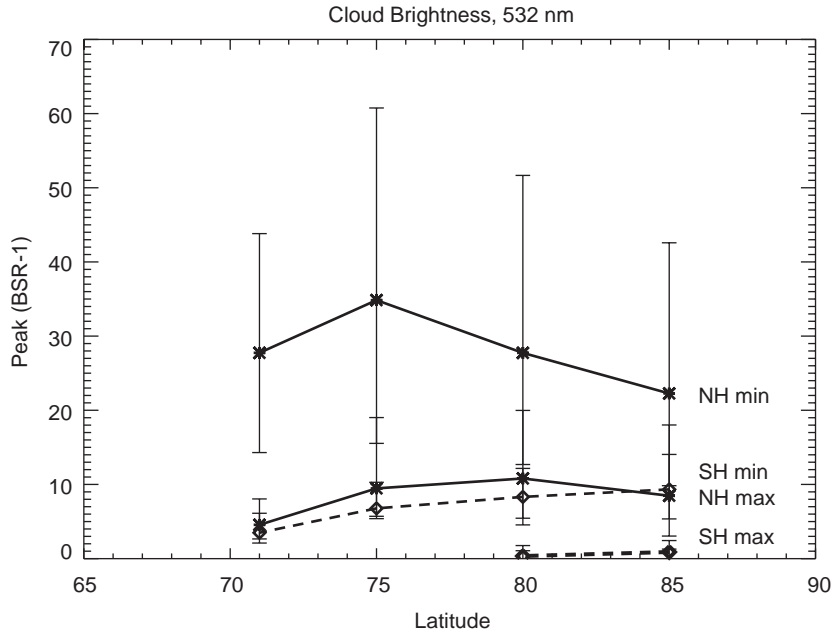


Fig. 8. Variation of the maximum BSR minus one ($BSR - 1$) as a function of absolute latitude. The solid lines are for the NH, and the dashed lines are for the SH. The labels “max” and “min” refer to solar maximum and solar minimum conditions, respectively. In the SH, for solar maximum, only clouds at 80° and 85° are shown since the model did not make a significant cloud at 71° or 75° . Here, the error bars simply give the minimum and maximum values of $(BSR - 1)$ for the last 3 days of each 4-day CARMA simulation.

It is currently difficult to validate our calculated N–S brightness asymmetry because of the relative lack of long-term comprehensive ground-based data sets at equivalent latitudes in both hemispheres. Preliminary first evidence from Rothera at 68°S (Chu et al., 2004) suggests fewer and dimmer clouds than at equivalent latitudes in the NH; however, the authors caution that this result may reflect limited sampling due to bad weather. Fiedler et al. (2003) compared BSR values at the SP with sub-polar NH data and found the SP data to be brighter, despite the fact that the SP data were obtained near solar maximum. If true, it is consistent with the suggestion we made in discussing the calculated cloud altitudes, namely, that our model overestimates the N–S difference.

For solar cycle variations, it is even more difficult to validate our model results since the available literature generally gives results in terms of frequency of occurrence rather than brightness. It is impossible to capture occurrence frequency variability in the model since it does not simulate meteorological variability. We do however have a suggestion below for how observers might correct for occurrence frequency so as to better compare with our model. Fiedler et al. (2003) suggest a factor of two decrease in brightness from 1997 to 2000 which might be solar cycle related. Clearly, more data will allow for better validation of our model result.

Fig. 9 shows the calculated albedo for a wavelength of 252 nm and a scattering angle of 120° . This is a typical wavelength and scattering angle from the SBUV instrument (DeLand et al., 2003). The figure also uses the same albedo definition as used by the SBUV instrument (scattered radiance ($\text{W}/\text{cm}^2/\text{nm}/\text{sr}$) divided by the spectral solar irradiance ($\text{W}/\text{cm}^2/\text{nm}$)). The figure shows a much a larger UV albedo in the NH relative to the SH and increases in both hemispheres for solar minimum. The solar cycle variation is about a factor of 2–3 in the NH, but is larger, about an order of magnitude or more, in the SH. Again, this is due to the more marginal temperatures for PMC formation in the SH. The model N–S difference is of the correct sign as the SBUV data, but appears to be too big in magnitude.

Finally, we should note that, at first glance, the overall model visible cloud brightness and UV albedo are much less than observations. For example, the peak BSR’s of 10–30 in the NH might be compared to the 40–100 reported by von Zahn et al. (1998). A similar discrepancy is also apparently seen in the UV albedo relative to SBUV. We argue that these apparent model-data discrepancies would be significantly reduced if one considered the fractional occurrence frequency in the observations. The model essentially assumes 100%, whereas at 69°N , the occurrence frequency is rarely as high as 50% and often as low as 20% (Fiedler et al., 2003). At the poles, the occurrence frequency is known

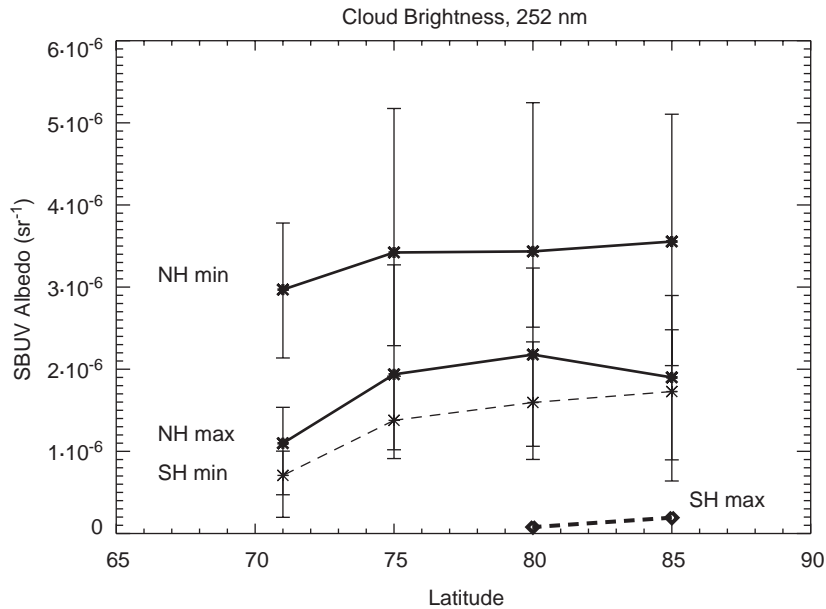


Fig. 9. Variation of the calculated UV albedo from CARMA. The wavelength is 252 nm which corresponds to the wavelength used by DeLand et al. (2003). The albedo is expressed in sr^{-1} to correspond to the units used by the SBUV satellite (see text). The error bars are the extrema of the calculated albedo, analogous to Fig. 8.

to be higher (Thomas and Olivero, 1989); however, a reliable estimate of the peak BSR and UV albedo at the poles is not yet available. We suggest, however, that in order to compare with our zonal mean results, that cloud observers consider combining their observables with the fraction of occurrence. Thus, clouds with peak BSR of 20 that are observed 40% of the time might be considered to have a zonal mean BSR of $0.4 \times 20 = 8$. Other combinations are possible, for example, one might consider a spectrum of occurrence frequencies convolved with a spectrum of BSR or albedo values.

Fig. 10 summarizes the calculated ratios of solar minimum to solar maximum for the four latitudes and three key parameters, visible peak BSR (from Fig. 7), UV albedo (from Fig. 8) and equivalent ice content (from Fig. 5). The figure clearly shows a greater solar cycle change in the SH relative to the NH. Also, the optical cloud signatures vary by more than $\text{H}_2\text{O}(\text{ice})$ because of a stronger dependence upon particle size which also changes from solar minimum to solar maximum.

In general, it appears that the solar cycle variation we calculate is greater than what is observed. Thus, we predict a factor of 5 change in 532 nm BSR – 1 at 71°N ; Fiedler reports no more than a factor of 2. We predict UV albedo changes of 2.7 at 71°N and a factor of 9.0 at the SP (infinity at 71°S). These are almost certainly more than the observed changes. Three factors could contribute to this. First, if the temperatures in the atmo-

sphere were lower than the 2D model output, PMC formation would be less marginal and thus less sensitive to perturbations from the solar cycle. Related to this is the fact that our zonal mean model does not capture the perturbations to the temperature such as tides or planetary waves (Kirkwood and Stebel, 2003) which could lower the temperature below the average and allow clouds to occur some fraction of the time. In this sense, our averaged model may underestimate the ability of the upper mesosphere to produce clouds. Certainly, as noted by one of the reviewers, the present model does not produce average PMC, but PMC representative for average atmospheric conditions. Second, horizontal transport of PMCs from higher latitudes could be the reason that PMCs are seen at 71°S and this is not in the current model.

The final possible factor is that the 2D model may overestimate the solar cycle variation of the mesopause temperature. We have searched for additional evidence that this is the case and the results are ambiguous. There is very little data on solar cycle temperature variations for the conditions where PMC are seen. Most of the relevant data are taken from OH^* nightglow data which are not available in the long summer twilights (see the review by Beig et al., 2003). Lübken and von Zahn (1991) discuss solar cycle variations in the upper mesosphere, but excluded summer measurements because of limited sampling. Clearly, this is an area which needs more data.

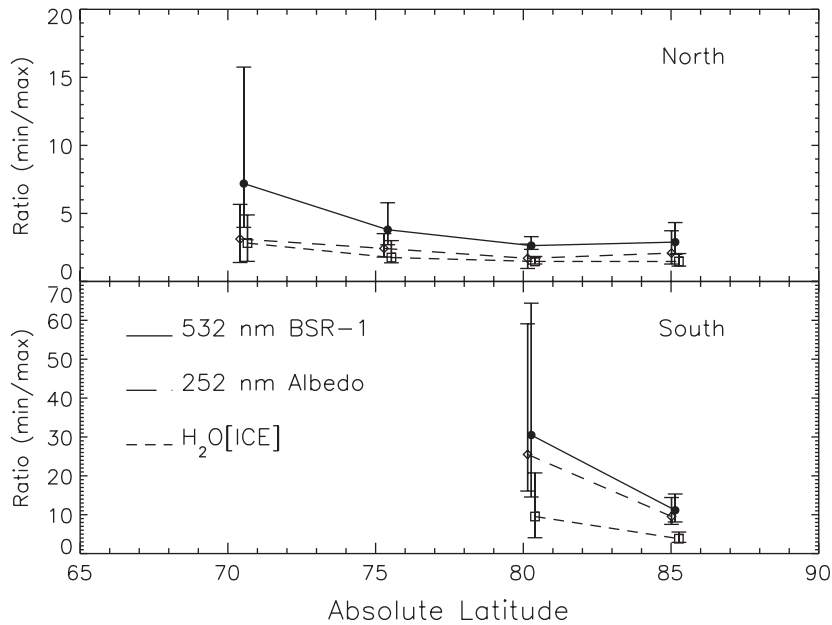


Fig. 10. Modeled solar cycle cloud variation of three cloud parameters vs. absolute latitude. The top panel is for the NH, and the bottom is for the SH. In each panel, the solid line is (BSR – 1) (see Fig. 8), the long dashed line is UV albedo (see Fig. 9) and the short dashed line is peak $\text{H}_2\text{O}(\text{ice})$ (see Fig. 6). As with Figs. 8 and 9, the error bars represent the minimum and maximum values in the last 3 days of the 4-day CARMA simulation.

4. Conclusions

Our results illustrate how the study of mesospheric clouds can be a diagnostic of mesospheric climate and variability. Specifically, we used calculated cloud parameters such as ice content, altitude and brightness and quantified the variability of these parameters as a function of hemispheric differences, solar cycle variations and latitudinal variability in mesospheric climate. Our main conclusions about cloud variability and mesospheric climate are as follows:

(1) In apparent agreement with observations, we find fewer and dimmer clouds in the SH relative to the NH. In our model, this is most directly because the Southern upper mesosphere is warmer than the Northern upper mesosphere by 5–10 K. This also appears to agree with the Pan and Gardner (2003) observations of SH mesopause temperatures rarely falling below 140 K at the SP, while high latitude NH temperatures below 130 K are routinely seen. However, it appears to disagree with the conclusion of Lübken et al. (1999) of hemispherically symmetric summer mesopause temperatures, although their error bars of 3 K are close to the model uncertainty in this conclusion. It also appears that the model overestimates the brightness differences between NH and SH clouds. This may mean that the model overestimates the asymmetry between NH and SH upper mesospheric temperatures.

(2) Our calculated clouds are of 2–3 km higher altitude in the SH relative to their counterparts in the NH. In our model, it results from a higher altitude of the 151–153 K isotherm in the SH relative to the NH. Qualitatively, this difference is in generally good agreement with lidar and satellite observations of PMCs, and thus supports the idea that there is a real difference in the temperature profile between the NH and SH. As was the case with the brightness variations, the observed altitude differences are less than the model differences. We also predict a solar cycle variation in cloud altitude with higher clouds at solar maximum. This may have already been observed in recent lidar data (Fiedler et al., 2003).

(3) Finally, a logical consequence of the argument for a warmer SH is that MC formation is more marginal in the SH and thus more sensitive to small temperature changes, for example, due to solar activity. A hemispheric difference in the solar response has not yet been reported; however, in principle, a reanalysis of the existing HALOE and SBUV databases could search for such an effect. The modeled solar cycle changes in PMC brightness are in the range of a factor of 3–7 for the NH (depending upon parameter) and over an order of magnitude in the SH. These numbers seem to lie at the high end of what is observed. However, the comparison of modeled solar cycle changes with observations are complicated by changes in the occurrence frequency which cannot be captured by our zonally averaged model. Even with that caveat in mind, it does appear

that the model changes are larger than the observed changes.

In summary, using the cloud variations as diagnostic of mesopause climate, our model/data comparison suggests that the model overestimates N–S differences in this climate as well as the solar cycle variation in this climate. Interestingly, if PMC formation itself were associated with heating either of the particles or of the atmosphere, it might be a negative feedback to solar cycle changes and could also act to reduce the calculated N–S differences. It has been suggested that PMC absorption of terrestrial IR radiation could be important (Espy and Jutt, 2002). We are also pursuing the possibility of photochemical feedbacks associated with the occurrence of PMCs due to ozone perturbations on the radiative budget. Since there are more PMCs in the NH or at solar minimum generally, the negative feedback would be greater at those times. Neither of these effects are in the current model; to include them would properly require an interactive PMC calculation which was coupled to CHEM2D. This is the subject of current research.

Acknowledgments

Funding for this work came from the Office of Naval Research and from the NASA Living With a Star program.

References

- Beig, G., et al., 2003. Review of mesospheric temperature trends. *Reviews of Geophysics* 41 (4), 1015.
- Berger, U., von Zahn, U., 2002. Icy particles in the summer mesopause region: three dimensional modeling of their environment and two-dimensional modeling of their transport. *Journal of Geophysical Research* 107 (A11), 1366.
- Bohren, C.F., Huffman, D.R., 1983. *Absorption and Scattering of Light by Small Particles*. Wiley, New York.
- Carbary, et al., 1999. Altitudes of polar mesospheric clouds observed by a middle ultraviolet imager. *Journal of Geophysical Research* 104, 10089–10100.
- Chou, M.-D., Suarez, M.J., 2002. A solar radiation parameterization for atmospheric studies, NASA Technical Memorandum 10460, vol. 15, 52pp.
- Chou, M.-D., Suarez, M.J., Liang, X.Z., Yan, M.-H., 2001. A thermal infrared radiation parameterization for atmospheric studies, NASA Technical Memorandum 104606, vol. 19, 65pp.
- Chu, X., Gardner, C.S., Papen, G., 2001. Lidar observations of polar mesospheric clouds at South Pole: seasonal variations. *Geophysical Research Letters* 28, 1203.
- Chu, X., Gardner, C.S., Roble, R.G., 2003. Lidar studies of interannual seasonal, and diurnal variations of polar mesospheric clouds at the South Pole. *Journal of Geophysical Research* 108 (D8), 8447.
- Chu, X., et al., 2004. Lidar observations of polar mesospheric clouds at Rothera, Antarctica (67.5S, 68.0W). *Geophysical Research Letters* 31, L02114.
- DeLand, M.T., Shettle, E.P., Thomas, G.E., Olivero, J.J., 2003. Solar backscattered ultraviolet (SBUV) observations of polar mesospheric clouds (PMCs) over two solar cycles. *Journal of Geophysical Research* 108 (D8), 8445.
- Espy, P.J., Jutt, H., 2002. Equilibrium temperature of water–ice aerosols in the high-latitude summer mesosphere. *Journal of Atmospheric and Solar-Terrestrial Physics* 64, 1823–1832.
- Fiedler, J., Baumgarten, G., von Cossart, G., 2003. Noctilucent clouds above ALOMAR between 1997 and 2001: occurrence and properties. *Journal of Geophysical Research* 108 (D8), 8453.
- Fogle, B., Haurwitz, B., 1966. Noctilucent Clouds. *Space Science Review* 6, 278–339.
- Fomichev, V.I., Blanchet, J.P., Turner, D.S., 1998. Matrix parameterization of the 15 μ m CO₂ band cooling in the middle and upper atmosphere for variable CO₂ concentration. *Journal of Geophysical Research* 103 (D10), 11505–11528.
- Gadsden, M., 1998. Noctilucent clouds seen at 60°N: origin and development. *Journal of Atmospheric and Solar-Terrestrial Physics* 60, 1763–1772.
- Garcia, R.R., 1989. Dynamics, radiation and photochemistry in the mesosphere: implications for the formation of noctilucent clouds. *Journal of Geophysical Research* 94, 14,605.
- Hervig, M., McHugh, M., Summers, M.E., 2003. Water vapor enhancement in the polar summer mesosphere and its relationship to polar mesospheric clouds. *Geophysical Research Letters* 30, 2041.
- Kirkwood, S., Stebel, K., 2003. Influence of planetary waves on noctilucent cloud occurrence over NW Europe. *Journal of Geophysical Research* 108, 8440.
- Lean, J., Rottman, G., Kyle, H.L., Woods, T.N., Hickey, J.R., Puga, L.C., 1997. Solar irradiance variability at 200–400 nm. *Journal of Geophysical Research* 102, 29939–29956.
- Lübken, F.-J., 1999. Thermal structure of the Arctic summer mesosphere. *Journal of Geophysical Research* 104, 9135–9149.
- Lübken, F.-J., Mullemann, A., 2003. First in situ temperature measurements in the summer mesosphere at very high latitudes. *Journal of Geophysical Research* 108 (D8), 8448.
- Lübken, F.-J., von Zahn, U., 1991. Thermal structure of the mesopause region at polar latitudes. *Journal of Geophysical Research* 96, 20841.
- Lübken, F.-J., Fricke, K.-H., Langer, M., 1996. Noctilucent clouds and the thermal structure near the Arctic mesopause in the summer. *Journal of Geophysical Research* 101 (D15), 9489–9508.
- Lübken, F.-J., Jarvis, M.J., Jones, G.O.L., 1999. First in situ temperature measurements at the Antarctic summer mesopause. *Geophysical Research Letters* 24, 3581.
- Marsh, D., Smith, A., Noble, E., 2003. Mesospheric ozone response to changes in water vapor. *Journal of Geophysical Research* 108 (D3), 4109.
- McCormack, J.P., 2003. The influence of the 11-year solar cycle on the quasi-biennial oscillation. *Geophysical Research Letters* 30, 2162.

- Pan, W., Gardner, C.S., 2003. Seasonal variations of the atmospheric temperature structure at South Pole. *Journal of Geophysical Research* 108, 4564.
- Rapp, M., Lübken, F.-J., Mullemann, A., Thomas, G.E., Jensen, E.J., 2002. Small-scale temperature variations in the vicinity of NLC: experimental and model results. *Journal of Geophysical Research* 107 (D19), 4392.
- Siskind, D.E., 2000. On the coupling between middle and upper atmospheric nitric oxide. *Atmospheric Sciences Across the Stratopause*, AGU Monograph, 2000, 342pp.
- Siskind, D.E., Eckermann, S.D., McCormack, J.P., Alexander, M.J., Bacmeister, J.T., 2003. Hemispheric differences in the temperature of the summertime stratosphere and mesosphere. *Journal of Geophysical Research* 108, 4051.
- Stevens, M.H., Englert, C.R., DeLand, M.T., Hervig, M., 2004. The polar mesospheric cloud mass in the Arctic summer. *Journal of Geophysical Research*, in press.
- Sugiyama, T., Muraoka, Y., Sogawa, H., Fukao, S., 1996. Oscillations in polar mesospheric summer echoes and bifurcation of noctilucent cloud formation. *Geophysical Research Letters* 23, 653–656.
- Summers, M.E., Siskind, D.E., Bacmeister, J.T., Conway, R.R., Zasadil, S., Strobel, D.F., 1997. Seasonal variation of middle atmospheric CH₄ and H₂O with a new chemical–dynamical model. *Journal of Geophysical Research* 102, 3503–3526.
- Thomas, G.E., 1991. Mesospheric clouds and the physics of the mesopause region. *Reviews of Geophysics* 29, 553–575.
- Thomas, G.E., 1996. Global change in the mesosphere–lower thermosphere region: has it already arrived? *Journal of Atmospheric Solar-Terrestrial Physics* 58, 1629–1656.
- Thomas, G.E., Olivero, J.J., 1989. Climatology of polar mesospheric clouds, 2. Further analysis of Solar Mesospheric Explorer data. *Journal of Geophysical Research* 94, 14673–14702.
- Thomas, G.E., Olivero, J.J., Jensen, E.J., Schroder, W., Toon, O.B., 1989. Relation between increasing methane and the presence of ice clouds at the mesopause. *Nature* 338, 490–492.
- von Cossart, G., Fiedler, J., von Zahn, U., 1999. Size distributions of NLC particles as determined from 3-color observations of NLC by ground-based lidar. *Geophysical Research Letters* 26 (11), 1513–1516.
- von Zahn, U., 2003. Are noctilucent clouds truly a “miner’s canary” for global change? *EOS* 84 (28), 261.
- von Zahn, U., Berger, U., 2003. Persistent ice cloud in the midsummer upper mesosphere at high latitudes: three-dimensional modeling and cloud interaction with ambient water vapor. *Journal of Geophysical Research* 108 (D8), 8451.
- von Zahn, U., von Cossart, G., Fiedler, J., Rees, D., 1998. Tidal variations of noctilucent clouds. *Geophysical Research Letters* 25, 1289.
- Woodman, R.F., et al., 1999. First observations of polar mesosphere summer echoes in Antarctica. *Journal of Geophysical Research* 104, 22577–22590.